ELSEVIER

PII: S0032-3861(98)00163-3

*Polymer* Vol. 39 No. 25, pp. 6391–6400, 1998

0032-3861/98/$ - see front matter

# Orientation of plane strain-compressed ultra-high-molecular-weight polyethylene

**Y. Boontongkong[a], R. E. Cohen[b,*], M. Spector[c,d] and A. Bellare[c,d]**
[a]*Department of Materials Science and Engineering, Massachusetts Institute of Technology, Cambridge, MA 02139, USA*
[b]*Department of Chemical Engineering, Massachusetts Institute of Technology, Cambridge, MA 02139, USA*
[c]*Department of Orthopedic Surgery, Brigham and Women's Hospital, Harvard Medical School, Boston, MA 02115, USA*
[d]*Rehabilitation Engineering R&D Laboratory, Brockton/West Roxbury VA Medical Center, West Roxbury, MA 02132, USA*
*(Received 11 December 1997; revised 26 January 1998; accepted 12 February 1998)*

Ultra-high-molecular-weight polyethylene (UHMWPE) samples of molecular weight 6 million were compressed using a channel die and characterized by wide-angle and small-angle X-ray scattering. The results were compared to previous studies performed on high-density polyethylene (HDPE) under the same compression conditions. Most deformation mechanisms exhibited by UHMWPE were also observed in HDPE. However, the onset of crystallographic and morphological orientation occurred at lower compression ratios in UHMWPE than in HDPE. Greater resistance to deformation and more extensive strain recovery were also exhibited by UHMWPE. These differences in deformation behaviour of UHMWPE and HDPE were attributed to the larger number of tie molecules and higher degree of entanglement within the amorphous regions of UHMWPE—a direct effect of its very high molecular weight. Our results clearly demonstrate that crystallographic texturing in UHMWPE, especially molecular orientation along the flow direction, can be controlled by channel die compression. This renders the method suitable for production of oriented samples for future studies of possible relationships between crystallographic texture and wear behaviour. 

**(Keywords: ultra-high-molecular-weight polyethylene; orientation; compression)**

## INTRODUCTION

### *Motivation*

Ultra-high-molecular-weight polyethylene (UHMWPE) is currently used as a bearing surface in total joint replacement prostheses. Superior toughness and wear properties of UHMWPE among various thermoplastics are generally attributed to its very high molecular weight, often in the range of several million grams per mole. However, prolonged functioning inside a patient's body produces polyethylene wear debris that stimulates biological response, which often results in loss of bone leading to loosening of the prosthesis and other complications. Such undesirable effects provide a driving force to improve the wear performance of UHMWPE. The material currently used for artificial joints undergoes no orientation processing designed to specifically maximize wear performance.

We believe that molecular and morphological orientation may influence the wear behaviour of UHMWPE such that wear properties could be optimized through appropriate processing. Certainly, a better knowledge of the relationship between wear properties and the material structure is necessary. We wished to establish a controlled method for texturing UHMWPE and to design appropriate means for characterization of the oriented polymer. A previous study[1] showed that channel die compression induced quasi-single crystallographic texture in high-density polyethylene (HDPE). Therefore, we chose channel die compression as the method to induce texture in UHMWPE.

Another motivation for our study derived from the existing knowledge of deformation-induced texture development of HDPE. Extensive studies of HDPE deformation have been performed by our research group, particularly under plane strain compression[1]. UHMWPE is the higher-molecular-weight version of polyethylene, rendering itself a suitable material for an extension of the previous studies.

### *Background*

Deformation-induced texturing to enhance mechanical properties of HDPE has been used for a variety of applications such as fibre and film drawing. These applications have provided the driving force for a number of experimental studies on HDPE under various deformation modes. The mechanisms underlying plastic deformation of semicrystalline polymers have been reviewed by Bowden and Young[2] and Lin and Argon[3].

Plastic deformation of polyethylene occurs via a number of mechanisms: interlamellar shear and separation, crystallographic slip, twinning, and stress-induced martensitic transformation. A quasi-single crystal of HDPE obtained from plane strain compression was used as a macroscopic approximation to a single crystal to probe deformation resistance of specific crystallographic plastic deformation mechanisms[4]. The study showed that competition among

* To whom correspondence should be addressed

crystallographic deformation mechanisms exists. Individual crystalline deformation mechanisms were isolated and examined. The least resistant slip mechanism was determined to be the (100)[001] chain slip with a critical resolved shear stress (CRSS) of 7.2 MPa. The (100)[010] transverse and (010)[001] chain slips have CRSS values of 12.2 and 15.6 MPa, respectively. Other slip mechanisms, twinning, and martensitic transformation may be also be active, but only to a very small extent even at large deformation.

According to the extensive channel die compression study on HDPE by Galeski *et al.*[1], it was determined that interlamellar sliding, deformation of the amorphous component and the easiest deformation mechanism to initiate, was prominent only at low compression ratios. While this amorphous sliding began to 'lock' as molecular extension of tie molecules increased, intense activity of the (100)[001] chain slip mechanism was observed. This was followed by activation of the (100)[010] transverse slip. The dominant (100)[001] slip and the (100)[010] slip, working in cooperation with each other, eventually resulted in a monocrystal texture at a high compression ratio of 6.4. No other crystallographic deformation mechanisms were activated, except possibly (110) twinning towards the highest compression ratio of 12, where a trace of fibrillar texture was observed.

Due to both crystallographic and amorphous deformation mechanisms, normals to the originally randomly distributed lamellae were found to rotate towards the loading direction as the lamellae thinned down and stretched out. At the compression ratio of 3.13, the transformation in the lamellar morphology set in. It was concluded that a systematic widespread pinch-off of the stretched lamellae occurred as they became unstable due to the increasing interface stretching resistance. Fragmentation was then initiated by thickness irregularity within lamellae. Crystalline fragments then underwent shape change to reduce interface energy, causing rotation of the interface around the centres of the fragments. The transformation eventually led to reconstruction of a new long period along the flow direction.

Studies have been performed with the objective of enhancing the mechanical properties of UHMWPE by different processing techniques[5–9]. However, a relatively few number of studies have been conducted on the mechanisms underlying the deformation of UHMWPE. Kaito *et al.*[9] investigated the change in texture of UHMWPE induced by rolling using a combination of small-angle X-ray scattering (SAXS) and wide-angle X-ray diffraction (WAXD) pole figures. They reported the crystalline slippage of the (100) plane along the chain direction and an inclined lamellar orientation at high deformation. Our work also employed plane strain compression. We used channel die compression to probe deformation mechanisms of the material. Our previous report on HDPE[1] compressed under similar conditions allowed us to make direct comparisons of UHMWPE deformation behaviour with that of HDPE and provided a basis for analysing the results.

## EXPERIMENTAL

### *Material preparation*

The raw UHMWPE was obtained from Westlake Plastics (Lenni, PA, USA) as a circular, ram-extruded rod with a 2-inch diameter. The resin was manufactured by Hoechst Celanese Corporation (Hostalen GUR 4150HP). The molecular weight of 6 million has been determined by intrinsic viscosity measurement[10]. The melt flow index is essentially zero. A recrystallization procedure was performed to establish a standard unoriented initial texture for compression. The raw UHMWPE samples were heated to 160–170°C for 1 h in an oven, then slowly cooled over approximately 3 h down to room temperature.

### *Channel die and compression condition*

*Figure 1* illustrates the channel die used to perform the plane strain compression. The steel channel die built by Lin and Argon[11] has a channel dimension of 10.5 mm in width and 76.2 mm in length. Load was applied to a plunger of the same dimension. Heating slabs were used to maintain the desired elevated temperature of the system. The die was the same one used for the previous channel die compression study of HDPE by Galeski *et al.*[1].

Each recrystallized sample was machined to fit snugly inside the channel die. All sample-die contact surfaces were lubricated with Dow-Corning high-temperature bearing grease (medium consistency) to minimize friction. During each compression, the temperature of the sample was maintained at 80°C. Each sample was compressed at the fixed engineering strain rate of 0.0025 $s^{-1}$ until the desired compression ratio (CR), defined by the ratio of original height to the compressed height, was reached. The same conditions of temperature and strain rate were employed previously for the compression of HDPE[1]. We also note for clarity that engineering strain is defined as (CR − 1), whereas true strain is given by the quantity ln (CR).

Once deformed to a nominal compression ratio, the entire set-up was allowed to cool to room temperature while the nominal compression ratio was maintained. The sample was released from the die at room temperature. Unlike HDPE, UHMWPE exhibited very significant strain recovery upon release from the channel die. Instantaneous strain recovery (height expansion) was measured immediately upon load release, and each compressed sample was also monitored for long-term strain recovery. The series of compressed samples comprise the following nominal compression ratios: 1.4, 1.9, 2.3, 3.2, 4.0, 5.6, and a fractured sample having a compression ratio prior to fracture between 6 and 7. In this latter sample, fracture was marked by an abrupt drop in compression load and an intense sound. Multiple cracks and readily separated chunks of material were apparent in this specimen. Each compressed sample was machined into three thin slabs approximately 1.5 mm thick, corresponding to the three orthogonal directions of the

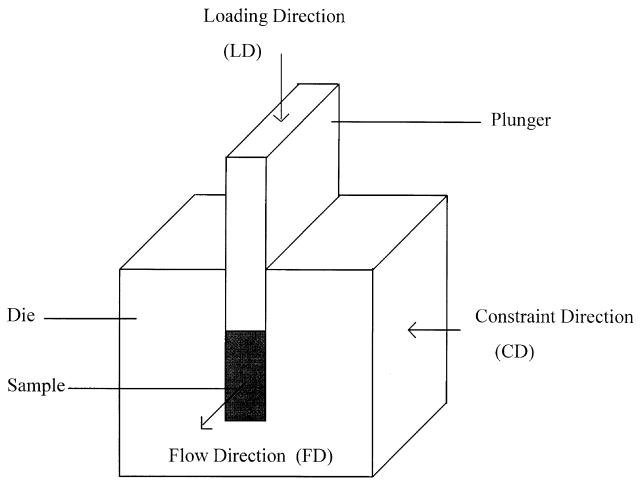


**Figure 1** Diagram of the channel die

channel die. These samples were used for subsequent X-ray analyses.

*Small-angle X-ray scattering (SAXS)*

The evolution of UHMWPE lamellar orientation was examined using SAXS measurements. Three separate instruments were used to perform the SAXS measurements. The majority of patterns included in this report were taken at the Center for Materials Science and Engineering, MIT, which operated with a Rigaku rotating-anode point source at 40 kV and 100 mA (or higher current). The beam was collimated by a cylindrical collimator; scattered X-rays travelled through an evacuated path to a 2D Siemens detector. The pattern of recrystallized standard was taken with a second instrument which operated with a Rigaku rotating-anode point source at 40 kV and 30 mA. The beam was collimated with the double-focusing Charles Supper mirrors; scattered X-rays travelled through a helium-filled cylindrical path to a 2D Siemens detector. These two instruments operated with Cu K$\alpha$ radiation of wavelength 1.54 Å. A few 1D scattering profiles were taken with an instrument at the National Synchrotron Light Source at Brookhaven National Laboratory (ultra-SAXS, beam line X23A3) which operated with a synchrotron source with 10 keV X-rays (wavelength 1.299 Å) and a moving detector. A desmearing procedure was used to obtained the final 1D profile with an ultra-low $q$-resolution of approximately 0.005 $nm^{-1}$; thus, scattering from large structure such as voids was observed. When the 2D instruments were used, integrated scattering curves were normalized and subtracted by their respective background curve according to Porod's extrapolation. In the case of ultra-SAXS, absolute intensity calibration obviated such assumptions.

The ideal purpose for a scattering experiment is to obtain the actual electron density profile which contains all the relevant information about the dimensions—e.g. long period, crystallite thickness, interfacial thickness—within a sample. To transform the experimental scattering profile $I(q)$ into the desired real-space pair distribution function $P(x)$, which is the same as the correlation function in the case of lamellar morphology, the following relation is required:

$$P(x) = 1/(2\pi^2 A)\left[\int_0^\infty q^2 I(q)\cos(qx)\,dq\right]$$

where $q = (4\pi \sin\theta/\lambda)$ is the scattering vector; $2\theta$ and $\lambda$ are the scattering angle and the radiation wavelength, respectively.

However, it is not possible to obtain a scattering curve that starts from $q = 0$, limited by the ability to resolve the data near the primary beam, nor is it possible to obtain data with a tail that extends to $q = \infty$, limited by the detector size and noise. Instead, we resorted to the simple Bragg's scattering analysis, $d = (2\pi/q)$, to estimate the most probable value of the long period spacing. The long period was estimated from the location of the peak of the plot of $Iq^2$ as a function of $q$, which takes into account the theoretical correction that lamellae are infinitely large in two directions[12].

*Pole figure*

The pole figure, a stereographic projection, was employed as the method to map the 3D crystallographic texture with respect to the compression geometry[13]. A Rigaku X-ray diffractometer operating with Cu K$\alpha$ X-rays of wavelength 1.54 Å was employed. The X-ray point source was generated by a rotating anode at 50 kV and 60 mA; the beam was filtered with an Ni filter. A dedicated MicroVAX computer was used for pole figure attachment control and data collection.

Polyethylene forms orthorhombic crystals with the $a$, $b$ and $c$ unit cell parameters of 7.4, 4.93 and 2.54 Å respectively. Pole figures were constructed for the (200), (020) and (002) crystallographic planes. All measurements covered the projection of Euler angles of sample

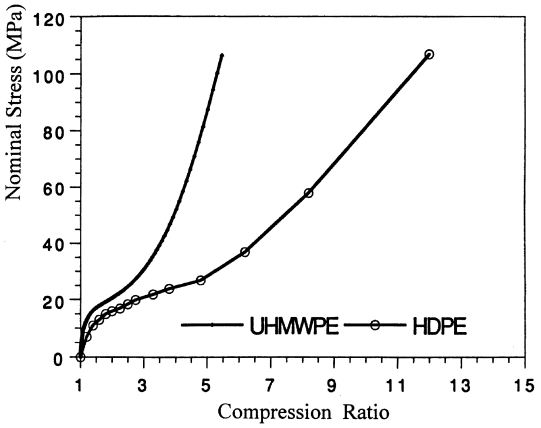


**Figure 2** Stress–compression ratio curves of channel die-compressed UHMWPE and HDPE

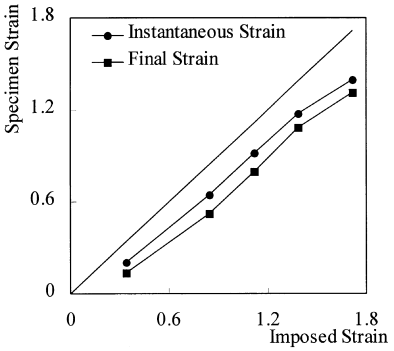


**Figure 3** Strain recovery plots of channel die-compressed UHMWPE

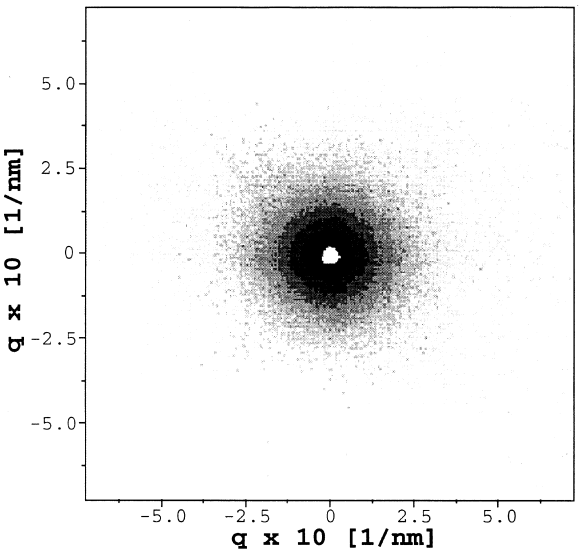


**Figure 4** SAXS pattern of unoriented standard sample

**Table 1** Degree of crystallinity determined using d.s.c.

| Sample | $\Delta H_{fusion}$ (J g$^{-1}$) | Crystallinity (%) |
|---|---|---|
| Standard (CR = 1) | 142.9 | 48.8 |
| CR = 1.4 | 143.1 | 48.9 |
| CR = 1.95 | 144.2 | 49.2 |
| CR = 3.2 | 131.7 | 44.9 |
| CR = 4.0 | 129.6 | 44.2 |
| CR = 5.6 | 124.9 | 42.6 |
| Fractured | 123.2 | 42.1 |

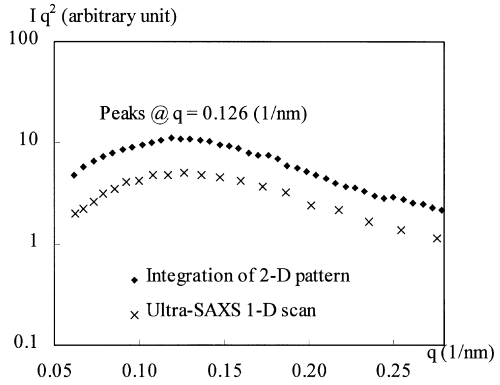


**Figure 5** Plots of $Iq^2$ *versus* $q$ of unoriented standard sample

orientation with respect to the incident beam: $\alpha$ from 0 to 90° and $\beta$ from 0 to 360°, both in 5° increments. The transmission-to-reflection connection angle for (200) and (020) measurements was 45°; the connection angle for (002) measurements was 30°.

To minimize the effects of sample geometry and X-ray absorption, two measurements were done to construct each pole figure. One measurement was done at the diffraction peak for the plane of interest ($2\theta$ angle determined by Bragg's law), the other at a $2\theta$ position a few degrees away from the peak as the background measurement. The peak intensity was corrected for the background intensity, then normalized to the background intensity. The normalized intensity was scaled from 0 to 10, then plotted into a finished pole figure. The center of each pole figure represents the flow direction (FD) of the channel die, while the vertical and horizontal directions correspond to the loading direction (LD) and the constraint direction (CD), respectively.

## RESULTS

### *Stress–compression ratio curves*

*Figure 2* illustrates the stress responses upon channel die compression of UHMWPE and HDPE under the same compression conditions: 80°C at a 0.0025 s$^{-1}$ strain rate. The prominent strain hardening exhibited by UHMWPE occurs much more abruptly than in HDPE. Compression ratio at fracture of UHMWPE is below 7, significantly lower than observed for HDPE (the ultimate compression ratios of both polymers are not shown in the *Figure 2*). Yielding in UHMWPE also occurs at a lower compression ratio than in HDPE.

### *Strain recovery*

*Figure 3* shows the strain recovery behaviour of channel die-compressed UHMWPE. The line of unit slope represents the case in which the strain in the material is identical to the strain imposed by compression. However, UHMWPE exhibited significant relaxation upon release from the die, resulting in an instantaneous reduction of strain relative to the imposed strain. Hence, the middle curve represents the true strains in the specimens immediately after load release. Each compressed UHMWPE sample also exhibited relaxation over extended time periods; the relaxation rate became negligible after approximately 2 months. The lowest curve represents the final true strains of compressed samples. Note that strain recovery in channel die-compressed HDPE was negligible and, therefore, was not reported in the previous study[1]. We found here that HDPE strain recovery was less than 10% of the magnitude of UHMWPE recovery, and persisted for less than 24 h.

### *Differential scanning calorimetry (d.s.c.)*

*Table 1* shows the degrees of crystallinity of the pre-compressed standard and the various compressed samples. The degree of crystallinity was determined based on the heat of fusion of 293 J g$^{-1}$ of linear polyethylene crystal[14]. The data showed a small increase in the degree of crystallinity at low compression ratios and a drop at higher compression ratios. The fractured sample shows approximately 7% lower crystallinity relative to the standard. Note that the degree of crystallinity of the standard sample was determined after the sample had been stored in the channel die at 80°C without being compressed to ensure the same thermal cycles as the compressed samples.

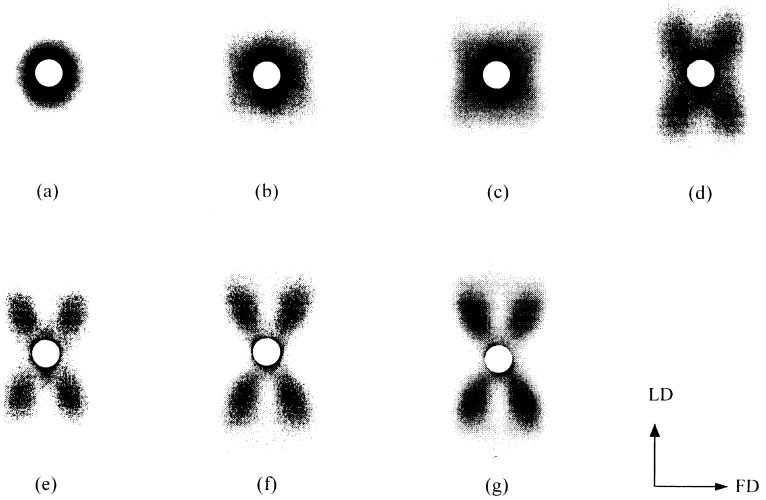


**Figure 6** SAXS patterns viewed along constraint direction (CD): (a) CR = 1.4; (b) 1.95; (c) 2.3; (d) 3.2; (e) 4.0; (f) 5.6; (g) fractured

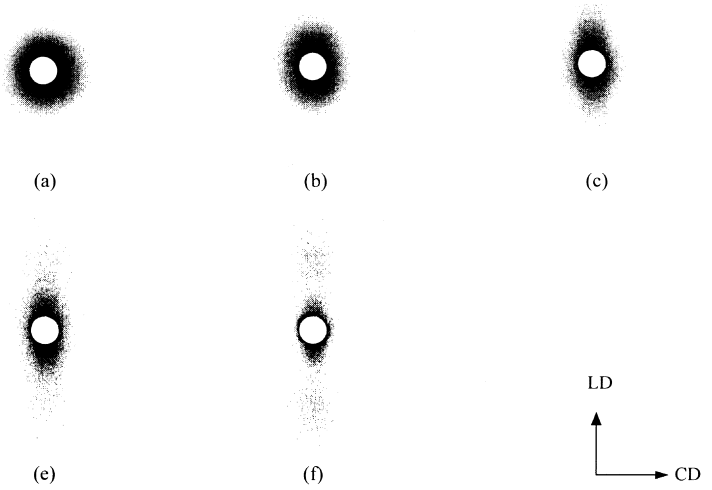


**Figure 7** SAXS patterns viewed along flow direction (FD): (a) CR = 1.4; (b) 2.3; (c) 3.2; (d) 4.0; (e) 5.6

*SAXS results*

*Figure 4* illustrates the isotropic SAXS pattern of the recrystallized uncompressed standard, which implies a randomly distributed lamellar structure. The $Iq^2$ *versus* $q$ plots of the standard sample obtained from integrated intensity of the pattern, as well as from the ultra-SAXS scan profile (*Figure 5*), yield a consistent estimate for an average long period spacing of 500 Å.

At the compression ratio (CR) of 1.4, the CD-view pattern (*Figure 6a*) shows a slight elongation of scattered intensity along LD. Integration of the pattern shows higher scattered intensity along LD than along FD. This indicates the start of rotation of lamellar normals towards LD, accompanied by thinning of the long period, in response to plane strain compression. The CD-view pattern at CR of 1.95 (*Figure 6b*) shows continued elongation of the pattern along LD. In addition, the pattern shows a trace of a developing four-point pattern. By the next higher CR of 2.3 (*Figure 6c*), the clear emergence of the four-point pattern is observed. At CR of 3.2 (*Figure 6d*) the lobes that constitute the four-point pattern have become the dominant characteristics of the CD-view pattern, while the scattered intensity along FD has noticeably reduced relative to that of the standard. Continued thinning of LD long period is confirmed by further elongation along LD of the FD-view pattern (*Figure 7c*).

The CD-view pattern at CR of 4.0 (*Figure 6e*) depicts further development of the four-point lobes orienting themselves approximately 28° to LD and a pair of less prominent vertical streaks near the primary beam. The pattern implies two lamellar populations: those with normals oriented at 28° to LD, and those with normals aligned along LD. The averaged long period spacing associated with the LD streaks obtained from the $Iq^2$ *versus* $q$ plot of ultra-SAXS scan along LD (*Figure 8*) is 370 Å, which is significantly larger than the 150 Å estimated long period obtained from the integrated intensity of the four-point lobes.

At CR of 5.6 (*Figure 6f*), the four-point lobes are the most prominent feature of the pattern. The lobes have become more radially extended, implying a wide distribution of long period spacings. Intensity integration of these lobes yield an estimate of the long period at 135 Å. The scattered intensity along FD is very low, essentially indicating the absence of lamellae whose normals align with FD at this high compression ratio. This CD-view pattern illustrates the drop in intensity of the streaks along LD relative to CR of 4.0, indicating a decrease in the population of lamellae with normals along LD. This is confirmed by the ultra-SAXS scans along LD (*Figure 9*) which show the drop in absolute intensity of the LD streaks located approximately at $q = 0.17\ \mathrm{nm}^{-1}$ as CR increases from 4.0 to 5.6. There is evidence for void-scattering at very low $q$ values in *Figure 9*.

The fractured sample (*Figure 6g*), having compression ratio between 6 and 7, shows little if any further development of the morphology relative to the sample at CR 5.6. The LD-view patterns (*Figure 10*) show a monotonic decrease of scattered intensity with increasing compression ratio, indicating a continuing elimination of

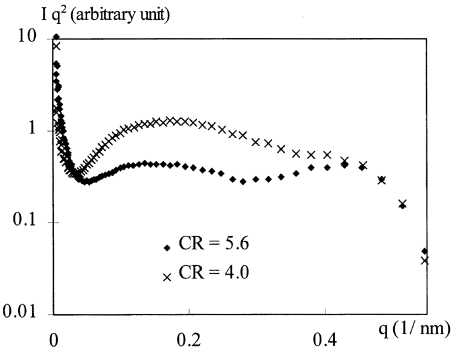


**Figure 8** Plots of $Iq^2$ *versus* $q$ obtained from ultra-SAXS scans along LD

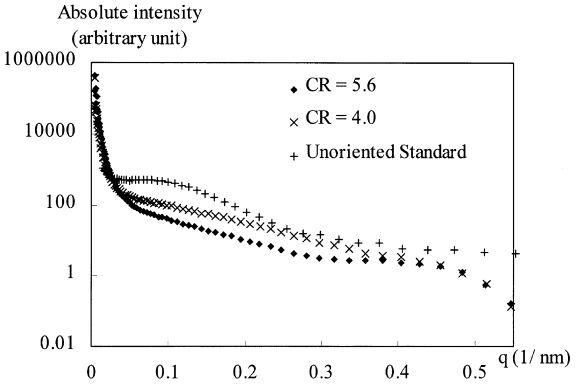


**Figure 9** Absolute intensity plots from ultra-SAXS scans along LD

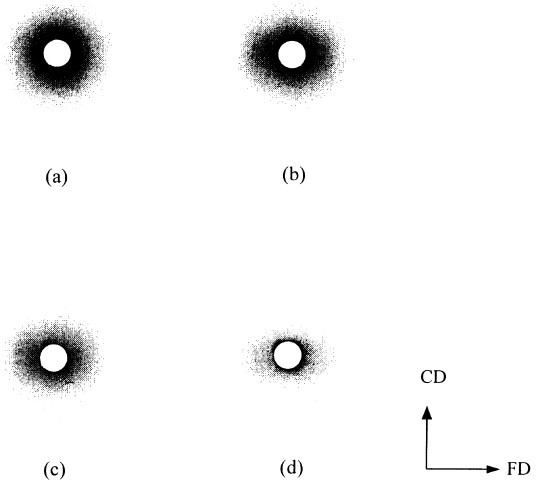


**Figure 10** SAXS patterns viewed along loading direction (LD): (a) CR = 1.4; (b) 1.95; (c) 3.2; (d) 5.6

lamellae aligned parallel to LD, particularly those with normals along CD.

*Pole figure results*

*Figures 11–16* illustrate the pole figures of the UHMWPE samples compressed to CR of 1.4, 1.95, 2.3, 3.2, 4.0 and 5.6, respectively. Even at the relatively low nominal CR of 1.4, a significant degree of crystallographic orientation is observed in the UHMWPE. The pole figure of the (002) plane normals shows that the normals to the (002) planes (the lamellar chain axes) have clustered towards FD along the LD–FD plane, while the pole figure of the (200) normals shows maximum along LD, both suggesting the activity of the dominant (100)[001] chain slip. The (020) plane normals cluster towards CD, indicating that the cooperative (100)[010] transverse slip has been already activated. Comparison of these pole figures to those of HDPE[1] shows that the UHMWPE texture at CR of 1.4 resembles that of HDPE compressed to CR of 1.55.

At CR of 1.95, the cooperative (100)[001] and (100)[010] slips account for the clustering of the (002) normals further towards FD, and the (020) normals rotating away from FD and towards CD. The UHMWPE crystallographic texture at

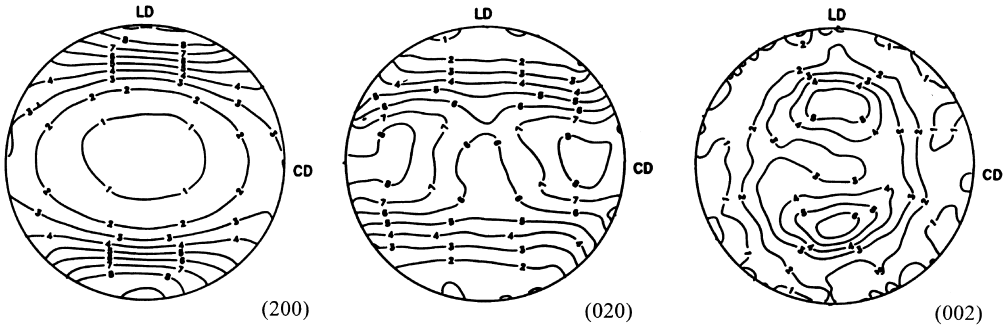


**Figure 11** Pole figures of normals to the (200), (020) and (002) planes; CR = 1.4

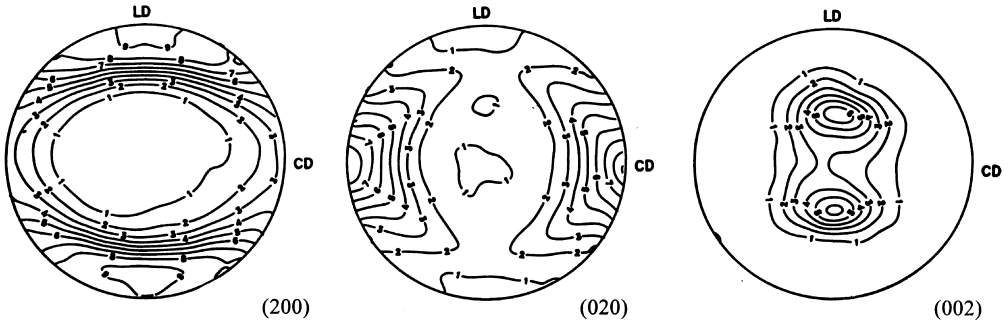


**Figure 12** Pole figures of normals to the (200), (020) and (002) planes; CR = 1.95

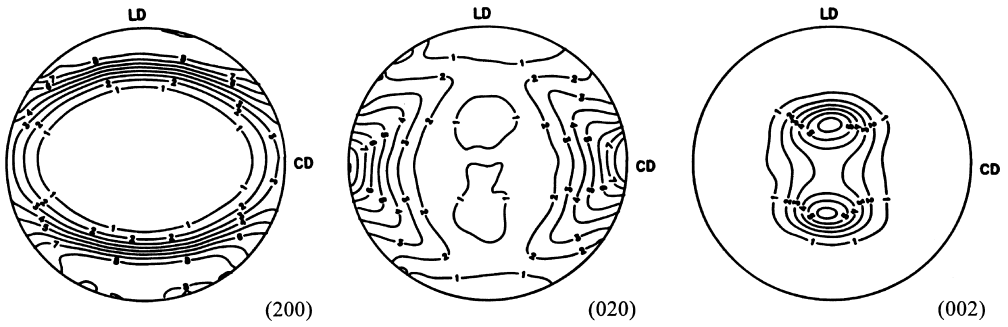


**Figure 13** Pole figures of normals to the (200), (020) and (002) planes; CR = 2.3

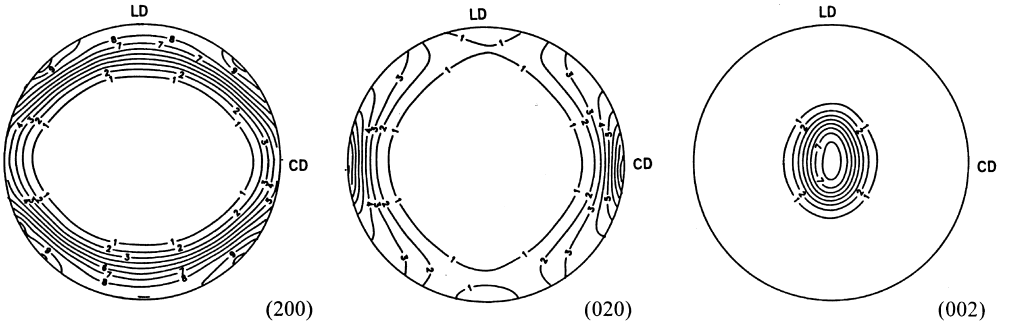


**Figure 14** Pole figures of normals to the (200), (020) and (002) planes; CR = 3.2

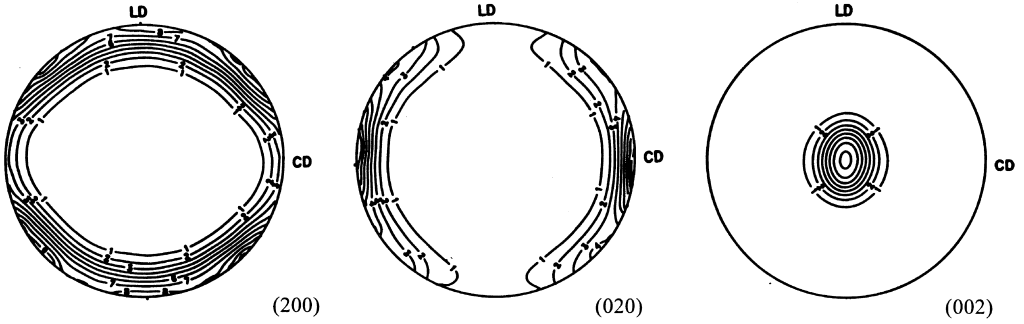


**Figure 15** Pole figures of normals to the (200), (020) and (002) planes; CR = 4.0

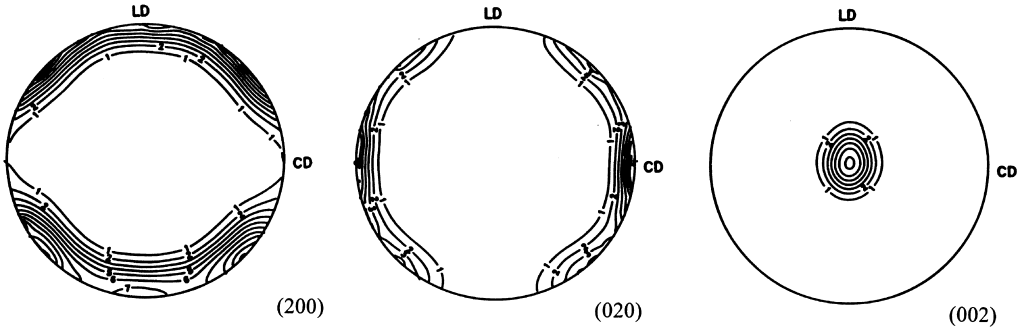


**Figure 16** Pole figures of normals to the (200), (020) and (002) planes; CR = 5.6

this CR correlates best to HDPE texture compressed to CR of 2.5. Note that the location of maximum clustering of the (200) plane normals has shifted by 20° towards FD, resulting in lower orientation of the (200) normals along LD. This implies 'locking' of interlamellar amorphous sliding, which is the coupling counterpart of (100)[001] chain slip. A similar effect of locking of amorphous shear was also observed in channel die-compressed HDPE.

The texture of UHMWPE at CR of 2.3 is comparable to the HDPE texture at CR of 3.13. It features more intensive clustering of the normals to (002) planes towards FD from LD, suggesting further activity of the (100)[001] dominant slip. The activity of the (100)[010] slip accounts for (020) pole figure evolution. The (200) normals cluster further towards LD as the location of absolute maxima shifts by 10° away from FD relative to the previous CR—an expected result of the (100)[001] slip. In addition, there is an onset of the (200) normal spreading towards CD, away from the LD–FD plane.

At CR of 3.2, the (200) plane normals evolve further away from FD, indicating continually increasing (100)[001] slip activity. Though the absolute maxima are located at 90° away from FD at this point, they have also moved away from LD to a position nearly half way between LD and CD. This marks a notable deviation of UHMWPE texture evolution from that of HDPE. Continuing on up to higher compression ratios, CRs of 4.0 and 5.6, the 'four-point' texture becomes the most prominent feature of the (200) pole figures: the absolute maxima eventually locate themselves at 45° between LD and CD. The intense activities of the (100)[001] slip and the cooperative (100)[010] slip are responsible for the texture evolution otherwise, evident by further clustering of the normals to the (200), (020) and (002) crystallographic planes towards LD, CD and FD, respectively. Note that there is an exceptional degree of chain alignment achieved along the flow direction in channel-die compressed UHMWPE at CR of 5.6.

## DISCUSSION

### *Comparison with HDPE*[1]

*Mechanical response.* Under the same compression conditions, strain-hardening in UHMWPE occurs much more abruptly, and fracture occurs at a much lower ultimate

compression ratio compared with HDPE. Yielding takes place at a lower compression ratio in UHMWPE than in HDPE. UHMWPE strain recovery occurs to a significantly larger extent and over a long time period, while HDPE does not exhibit significant strain recovery after compression. These features clearly indicate higher resistance to deformation of UHMWPE relative to HDPE.

*Morphological texture.* The clustering of lamellar normals towards LD in UHMWPE is observed at the early stages, which is expected as a result of amorphous shear and lamellar slip shear. While for HDPE, this morphological arrangement is the prominent response to the deformation up to the intermediate CR of 3.13, it is not the case for UHMWPE. The CD-view pattern of UHMWPE shows a faint four-point pattern emerging relatively early at CR of 1.95, superimposing onto the LD-elongated pattern. As the degree of deformation increases, the four-point pattern develops; the intensity increases, the shape evolves into well-defined lobes. A similar distinct four-point SAXS pattern was also observed in rolled UHMWPE by Kaito *et al.*[9]. The development of the four-point lobes occurs mainly at the expense of the lamellae whose normals originally align along FD and CD, evident from the decrease in scattered intensities along these directions. By CR of 4.0, two populations of clustered lamellar are observed: those with normals along LD which give rise to the LD streaks, and the lamellae with normals approximately at 28° to LD which give rise to the four-point lobes.

We postulate that the origins of the observed four-point pattern are lamellae that have undergone kinking in response to the deformation, forming a chevron (or herring-bone) lamellar morphology. As an indirect supporting evidence, this type of morphology was documented in an earlier study of HDPE by Song *et al.*[15] which included transmission electron micrographs of channel die-compressed samples depicting well-ordered kinked lamellar stacks, as well as the associated SAXS patterns consistent with the micrographs.

The four-point pattern in UHMWPE is azimuthally narrow (though significantly spread-out in the radial direction) and the azimuthal angle between two adjacent lobes is consistent. These features demonstrate that the kinked lamellae which give rise to the pattern are quite large and that their normals form a consistent angle of about 28° to LD. In contrast, the four-point pattern exhibited by HDPE[1] is relatively diffuse and transient: the pattern eventually transforms into a pair of arcs along FD. As concluded by Galeski *et al.*[1], the HDPE four-point pattern arises from fragmented lamellar blocks undergoing a morphological transformation leading to a new long period along FD. The fact that our compressed UHMWPE samples exhibit the development of well-defined four-point pattern up to the highest attainable degree of deformation (i.e. the fractured sample) indicates absence of such restructuring transformation in UHMWPE.

The long period obtained from the streaks along LD (at CR of 4.0) is significantly larger than the value obtained from the four-point pattern. This indicates that the kinked lamellae that have clustered to form the chevron morphology apparently underwent more extensive rotation and experienced more significant thinning than the LD lamellae. This and the relatively early formation of four-point pattern in UHMWPE compared to HDPE suggest a higher degree of restriction to rotation of UHMWPE lamellae towards LD relative to those of HDPE, and that only those lamellae whose normals were originally nearly parallel to LD manage to cluster towards LD without kinking.

*Crystallographic texture.* Comparison of UHMWPE and HDPE[1] pole figures shows that up to CR of about 2.3, the crystallographic texture evolution in plane strain-compressed UHMWPE can be correlated with that of plane strain-compressed HDPE. Therefore, similar to HDPE, we conclude that the crystallographic deformation mechanisms which contribute to the orientation are primarily the (100)[001] chain slip and, secondarily, the (100)[010] transverse slip. However, the compressed UHMWPE texture correlates with a compressed HDPE sample of a higher compression ratio, implying earlier crystallographic orientation of UHMWPE with respect to that of HDPE. This tendency for UHMWPE to develop an oriented crystallographic texture at lower strains than HDPE was observed in our experiments despite the more extensive relaxation exhibited by compressed UHMWPE upon load release which probably caused some loss of orientation.

A noticeable difference in the evolution of UHMWPE crystallographic texture from that of HDPE in similar deformation arises near CR of 2.3, where the maxima in the pole figure of the (200) plane normals begin to move away from LD towards CD. With increasing compression ratios, these maxima eventually reside at a 45° angle between LD and CD, while secondary maxima occur along LD. This suggests that another deformation mechanism, possibly twinning or martensitic transformation working simultaneously with the two cooperative slips, is responsible for the unique 'four-point' texture of compressed UHMWPE. In comparison, the HDPE texture develops nearly monotonically towards that of a monocrystal up until the highest CR of 12, where a trace of fibrillar texture is observed in the (020) pole figure. The fibrillar texture observed in HDPE forms at a relatively high CR, while the 'four-point' texture observed in UHMWPE does not occur in HDPE.

*Analysis*

Even though HDPE has a higher degree of crystallinity (65%) compared to UHMWPE (49%) and though the basic crystallographic mechanisms of deformation are the same in both polymers, UHMWPE clearly exhibits higher resistance to plane strain compression than HDPE. It is evident, therefore, that the mechanical response of the amorphous regions in UHMWPE is dramatically different from that exhibited by the amorphous regions in HDPE. We attribute the difference in their mechanical response to the difference in the amount of unattached chain ends and the difference in the amount of tie molecules, i.e. molecules that are incorporated into multiple lamellae or ones that form trapped entanglements with molecules emanating from neighbouring lamellae[16].

For a given polyethylene sample of fixed molecular weight, the amount of tie molecules can be controlled to some extent by the crystallization process. Processes that facilitate for adjacent reentry of a chain back into the same lamella, such as solution crystallization, result in relatively few tie chains. On the other hand, such processes in which the ability for molecules to chain-fold is hindered result in a greater number of tie chains. As indirect evidence of the effects of number of tie molecules and degree of chain

folding, it has been observed that quench-crystallization of polyethylene resulted in enhanced toughness and strain hardening[16].

In our comparative examination of HDPE and UHMWPE, molecular weight is the main variable contributing to differences in the crystallization processes. Upon crystallization from the melts, the ability for larger molecules of UHMWPE to reptate is more hindered than for the smaller molecules of HDPE. Thus, UHMWPE molecules are more likely to be incorporated into multiple crystals than HDPE molecules. This is evident from the higher toughness and lower degree of crystallinity of UHMWPE relative to HDPE. One could expect a higher fraction of trapped entanglements within the amorphous regions of UHMWPE and better connectivity among lamellae in UHMWPE than in HDPE due to the large number of tie molecules and small number (essentially none) of loose chain ends.

In rationalizing the deformation behaviour of UHMWPE, it is useful to draw an analogy of our comparative systems to the well-established knowledge of the effect of primary chain (pre-crosslink) molecular weight on the deformation behaviour of elastomers[17]. The low-strain stiffness depends on the effective crosslink density which differs from the nominal chemical crosslink density by a factor $[1-(2M_c/M_o)]$, where $M_c$ is the average molecular weight between crosslink points (between trapped entanglements, in the present context) and $M_o$ is the primary chain molecular weight. In the analogy to the amorphous regions of our polyethylene samples, the value of $M_o$ for UHMWPE is effectively infinite, leading to the maximum possible stiffness for the amorphous regions of UHMWPE.

The virtual absence of loose chain ends and the larger fraction of trapped entanglements are, therefore, the most probable explanation for the stiffer and more easily 'locked' mechanical response exhibited by UHMWPE than by HDPE. Larger strain recovery of UHMWPE can be explained based on the fact that the oriented UHMWPE molecules are effectively incapable of undergoing any disentanglement upon deformation. Therefore, a larger amount of recoverable strain energy is stored by trapped entanglements.

The high trapped entanglement density, the high degree of connectivity, and the resulting higher stiffness of the amorphous regions of UHMWPE contribute to early activation of crystallographic slip mechanisms in UHMWPE. The absence of restructuring transformation observed at large deformation in HDPE is also a likely result of the exceedingly high molecular weight of UHMWPE which leads to a more topologically constrained structure incapable of fragmentation and subsequent reorganization. Strain hardening leads to macroscopic fracture of the material before this transformation, initiated by lamellar 'pinch-off' and 'combing-out' of defects, can occur. Finally, the early development of the lamellar kinking in UHMWPE arises because rotation of lamellar normals towards LD becomes restricted; kinking become necessary to accommodate further imposed strain.

## CONCLUSION

We are able to induce a near-monocrystal texture, including an exceptional molecular alignment along the flow direction, in UHMWPE using channel die compression. The previous HDPE study by Galeski *et al*.[1] provides a basis for comparison to the plane strain deformation behaviour of UHMWPE. The material exhibits greater resistance to deformation and more extensive strain recovery than HDPE. SAXS results indicate relatively early formation of a four-point pattern. Subsequent development of the well-defined four-point pattern is consistent with a hypothesis of lamellar kinking and formation of a chevron morphology. Unlike HDPE, UHMWPE lamellar morphology does not undergo a restructuring transformation even up until the point of fracture. From the pole figures, the relatively early onset of crystallographic orientation in UHMWPE is observed. Most of the mechanisms underlying the crystallographic evolution of HDPE are also responsible for the crystallographic texturing in UHMWPE

We attribute the difference in deformation behaviour of UHMWPE and HDPE mainly to the difference in their amorphous regions. The analogies drawn between the amorphous regions of the two materials and crosslinked elastomers are useful in rationalization of the deformation behaviour of UHMWPE. The very high molecular weight results in a large number of tie molecules and higher degree of trapped entanglement within the UHMWPE amorphous region. This direct effect of the high molecular weight accounts for higher resistance of the amorphous regions to plastic deformation and early texture evolution of UHMWPE relative to HDPE.

Wear tests are currently being performed on compressed specimens to examine wear rates of the three surfaces corresponding to the orthogonal directions of the channel die geometry. These results will be presented in future publications.

## ACKNOWLEDGEMENTS

This work was financially supported by the Office of Research and Development, Department of Veterans Affairs (VA), under grant number A877-RA. We thank Dr Z. Bartczak for his helpful discussions and Professor F. J. McGarry for the use of the Instron machine. Y. B. acknowledges his graduate scholarship from the Royal Thai government.

## REFERENCES

1. Galeski, A., Bartczak, Z., Argon, A. S. and Cohen, R. E., *Macromolecules*, 1992, **25**, 5705.
2. Bowden, P. B. and Young, R. J., *J. Mater. Sci.*, 1974, **9**, 2034.
3. Lin, L. and Argon, A. S., *J. Mater. Sci.*, 1994, **29**, 294.
4. Bartczak, Z., Argon, A. S. and Cohen, R. E., *Macromolecules*, 1992, **25**, 5036.
5. Han, K. S., Wallace, J. F., Truss, R. W. and Geil, P. H., *J. Macromol. Sci. Phys.*, 1981, **B19**, 313.
6. Smith, P., Chanzy, H. D. and Rotzinger, B. P., *Polymer Commun.*, 1985, **26**, 258.
7. Pawlikowski, G. T., Porter, R. S. and Mitchell, D. J., *J. Polym. Sci., Polym. Phys. Ed.*, 1988, **26**, 1865.
8. Wang, L.-H. and Porter, R. S., *J. Polym. Sci., Polym. Phys. Ed.*, 1990, **28**, 2441.
9. Kaito, A., Nakayama, K. and Kanetsuna, H., *J. Appl. Polym. Sci.*, 1983, **28**, 1207.
10. Li, S. and Burstein, A. H., *J. Bone Joint Surg. Am.*, 1994, **76A**, 1080.
11. Lin, L. and Argon, A. S., *Macromolecules*, 1992, **25**, 4011.
12. Russell, T. P., in *Handbook of Synchrotron Radiation*, Vol. 3, eds. G. S. Brown and D. E. Moncton. Elsevier, New York, 1991, Chapter 11.
13. Cullity, B. D., *Elements of X-ray Diffraction*, 2nd edn. Addison-Wesley, Reading, MA, 1978, Chapter 9.

14. Wunderlich, B. and Cormier, C. M., *J. Polym. Sci., Polym. Phys. Ed*. 1967, **5**, 987.
15. Song, H. H., Argon, A. S. and Cohen, R. E., *Macromolecules*, 1990, **23**, 870.
16. Knight, G. W., in *Polymer Toughening*, ed. C. B. Arends. Marcel Dekker, New York, 1996, p. 189.
17. Flory, P. J., *Principles of Polymer Chemistry*. Cornell University Press, Ithaca, NY, 1953, Chapter 11.